Monthly Notices
of the
ROYAL ASTRONOMICAL SOCIETY

MNRAS **459,** 357–365 (2016)
Advance Access publication 2016 March 23

doi:10.1093/mnras/stw680

Class I methanol megamasers: a potential probe of starburst activity and feedback in active galaxies

X. Chen,[1,2]★ S. P. Ellingsen,[3] J.-S. Zhang,[4] J.-Z. Wang,[2] Z.-Q. Shen,[1,2] Q.-W. Wu[5] and Z.-Z. Wu[6]

[1]*Key Laboratory for Research in Galaxies and Cosmology, Shanghai Astronomical Observatory, Chinese Academy of Sciences, 80 Nandan Road, Shanghai 200030, China*
[2]*Key Laboratory of Radio Astronomy, Chinese Academy of Sciences, Nanjing, JiangSu 210008, China*
[3]*School of Mathematics and Physics, University of Tasmania, Hobart, TAS, 7001 Australia*
[4]*Center for Astrophysics, GuangZhou University, Guangzhou 510006, China*
[5]*School of Physics, Huazhong University of Science and Technology, Wuhan 430074, China*
[6]*College of Science, Guizhou University, Guiyang 550025, China*

Accepted 2016 March 18. Received 2016 March 18; in original form 2016 February 2

ABSTRACT

Previous observations have shown that the distribution of 36.2-GHz class I methanol maser (MM) emission in Arp 220 is highly correlated with the diffuse X-rays. On this basis it was suggested that methanol MM may be produced either by the effects of galactic-outflow-driven shocks and/or cosmic rays. Here we report the results of a single-dish survey undertaken with the Greenbank Telescope (GBT) to improve our understanding of the pumping conditions of extragalactic class I methanol masers and their relationship to starburst and feedback processes within the host galaxies, towards a sample which includes 16 galaxies which show both extended soft X-ray emission, and either OH or H_2O MM emission. Large baseline ripples in the GBT spectra limited our results to tentative detections towards 11 of the target galaxies. Analysis of these tentative detections shows that there are significant correlations between the methanol intensity and the host-galaxy infrared, radio and OH MM emission, but no correlation with the X-ray and H_2O MM emission. Some sources show methanol emission significantly offset from the systemic velocity of the galaxy (by up to 1000 km s^{-1}) and we propose that these are associated with galactic-scale outflows from active galactic nuclei (AGNs) feedback. The combined observational properties suggest that class I methanol MMs are related to significant starburst and molecular outflow activity and hence may provide a potential probe of AGN feedback and starburst processes in the host galaxies.

Key words: masers – galaxies: ISM – galaxies: starburst – radio lines: ISM.

1 INTRODUCTION

Methanol is a commonly observed species in interstellar gas and it has a very rich spectrum of thermal and masing transitions at microwave and millimetre wavelengths. The large number of transitions has made it a powerful tool for investigating star formation activity in the Milky Way. More than 1000 methanol maser sources have been detected in our Galaxy (e.g. Green et al. 2009; Chen et al. 2014). Based on the different excitation environments and pumping conditions, methanol maser transitions are empirically divided into two classes, class I and class II (Batrla & Menten 1988; Menten 1991). Class I masers are collisionally pumped in regions where mildly shocked gas is driven into molecular clouds by outflows or expanding H II regions (e.g. Voronkov et al. 2010; Chen et al. 2011), while class II masers are pumped by infrared (IR) radiation from young high-mass stars (e.g. Ellingsen 2006; Caswell et al. 2010). In addition, both OH and H_2O masers are frequently observed towards high-mass star formation regions, and are often closely associated with class II methanol masers (e.g. Breen et al. 2010; Li et al. 2012).

Maser emission from the 1667 MHz OH and 22 GHz H_2O transitions has been detected in more than 100 active galaxies for both species (e.g. Darling & Giovanelli 2002; Zhang et al. 2012). In many of these sources the OH or H_2O maser emission has an isotropic luminosity more than a million times greater than that observed in typical Milky Way star formation region masers and because of this they are commonly referred to as megamasers. OH megamasers are usually associated with starburst nuclei in ultraluminous infrared galaxies (ULIRGs; e.g. Baan, Wood & Haschick 1982), while water megamasers are often associated with accretion discs and jets

★ E-mail: chenxi@shao.ac.cn

towards low-luminosity active galactic nucleus (AGN), typically Seyfert 2 or LINER galaxies (e.g. Miyoshi et al. 1995). Compared to the rich and active methanol maser phenomena observed in our Galaxy, to date, extragalactic methanol maser emission from either class I (at 36.2 GHz) or class II (6.7 or 12.2 GHz) transitions has only been detected in a few galaxies, specifically the Large Magellanic Cloud, M31 and NGC253 (Green et al. 2008; Ellingsen et al. 2010, 2014; Sjouwerman et al. 2010). The isotropic luminosity of typical methanol masers observed in Galactic star formation regions is around 10^{-5} $L_{\odot}$, and the methanol emission detected in nearby extragalactic sources is in all cases two or more orders of magnitude short of being a megamaser (i.e. >10 $L_{\odot}$).

Recently, significant advances have been made in searches for extragalactic class I methanol megamasers, with detections towards two galaxies – the major-merger galaxy Arp 220 has been detected in the 36.2-GHz class I transition (Chen et al. 2015), and the Seyfert galaxy NGC 1068 has been detected in the 84.5-GHz class I transition (Wang et al. 2014). Interferometric mapping observations of the 36.2-GHz methanol megamasers towards Arp 220 show that the methanol emission is highly correlated with the diffuse soft X-ray emission in this system. There have been two hypotheses proposed to explain this observation. One is that high-energy cosmic rays play a role in the enhancement of methanol emission abundance in these regions. This mechanism has been proposed as an explanation for the production of 36.2-GHz methanol masers in the central molecular zone of the Milky Way (Yusef-Zadeh et al. 2013) and NGC 253 (Ellingsen et al. 2014). The alternate hypothesis is that the X-ray plume in Arp 220 is the result of a starburst-generated superwind which results in a region associated with both rapidly outflowing and inflowing shock-heated gas. In this scenario the widespread shocks within the plume region are thought to be critical in producing widespread 36.2-GHz class I methanol emission. The observations of 36.2-GHz methanol emission in Arp 220 by Chen et al. (2015) also found that in contrast to OH and H_2O megamasers which originate close to the nucleus, the class I methanol megamasers are significantly offset from the nuclear region and show an extended spatial distribution with a scale of a few kpc. This suggests that the class I methanol megamasers trace feedback (e.g. outflows) and star formation processes on larger scales beyond the circumnuclear regions of starburst galaxies.

The limited observational information currently available for class I methanol megamasers means that further searches are required to clarify the pumping conditions (either outflow-driven shocks, cosmic rays or both) and to determine the role and significance of class I methanol megamasers for studies of starburst activity and feedback processes within the host galaxies. In order to address these questions we have undertaken a systematic survey with the National Radio Astronomy Observatory (NRAO) Greenbank Telescope (GBT) for 36.2-GHz class I methanol masers towards galaxies with extended X-ray emission which also show megamaser emission from water or OH. Extended X-ray emission may trace the physical environment of outflow-driven shocks or high-energy cosmic rays, allowing us to investigate these phenomena. In this paper, we report the results of this search.

2 SOURCE SAMPLE AND OBSERVATION

The limited observations of 36.2-GHz extragalactic methanol emission which have been made to date (Chen et al. 2015) suggest that galaxies with extended soft X-ray emission provide the physical conditions necessary to produce methanol megamasers. The observing sample is considered towards the extended X-ray galaxies which show megamaser emission from water or OH, since the detection rate of class I methanol masers should tend to be higher in sources with megamasers. The target sample for our survey includes eight water megamaser galaxies (among them two galaxies which also host OH megamasers) which also exhibit soft X-ray emission detected in *Chandra* and/or *XMM–Newton* observations (Zhang et al. 2006; Brassington, Ponman & Read 2007). In addition, we also include eight OH megamaser galaxies with extended X-ray emission detected in *ROSAT* observations (Kandalyan 2003). The two different sub-samples of water and OH megamaser galaxies considered in our observations also allow us to investigate whether there are differences between them in the characteristics of any detected methanol megamaser emission. The characteristics and important parameters of the sample sources are listed in Table 1.

The observations were made using the NRAO GBT over the period 2015 February 4–8. We use eight VEGAS spectrometers each of which has 1250-MHz effective bandwidth and a spectral resolution of 92 kHz, to make observations with two beams of the *Ka*-band receiver (four spectrometers for each beam). This spectral resolution corresponds to about 0.8 km s^{-1} at 36 GHz. The four spectrometers for each beam were configured with centre frequencies of 33.8, 34.8, 35.8 and 36.3 GHz to yield an instantaneous frequency coverage of 33.2–37 GHz, which allowed us to cover the sky-frequency of the $4_{-1} \rightarrow 3_0$ class I methanol transition (rest frequency 36.169 265 GHz) for all of the sources in the sample. This frequency configuration results in galaxies with a recessional velocity of less than 3000 km s^{-1} (including six sources; see Table 1) being observed in two of the four spectrometers (3 and 4), allowing us to cross-check for any correlator artefacts for these sources. The half-power beamwidth of the telescope was about 20 arcsec at this frequency. The aperture efficiency of the telescope is approximately 50 per cent, corresponding to a conversion factor of 0.7 Jy K^{-1} to represent the measured antenna temperature as a flux density. The observations were performed in switching mode, nodding between the two beams with a switching time of 1 min. The typical on-source integration time for each source was 1 h (obtained from the sum of the two beams for each source). The antenna pointing was checked and corrected before the observation of each target source. The typical pointing accuracy is estimated to be better than 4 arcsec. The system temperature was typically in the range 60–100 K during the observations, resulting in an rms noise level of about 1 mJy in the final spectrum (for a velocity resolution of $\sim$20 km s^{-1} – see below).

Data reduction was performed using the GBTIDL package. There was no significant Radio Frequency Interference (RFI) within the observed frequency range (33.2–37 GHz) for any of the target sources. The final spectra covering the entire observed frequency range from each spectrometer contain large-scale (typical frequency span >0.2 GHz $\sim$ 1150 km s^{-1}) non-periodic baseline ripples for most of the target sources. The large baseline ripples are likely due to the switching time used in the nodding between the two beams in our observations (1 min). GBT memo 246 recommends a switching time of less than 30 s for *Ka*-band observations to minimize baseline ripple.[1] Unfortunately we were not aware of this recommendation until after the observations were complete; however, it is clearly an important requirement for any follow-up observations of this transition with the GBT. Alternatively, observations with an interferometer are generally able to achieve better baseline calibration, so the Very Large Array (VLA) in D array might be the best

[1] http://www.gb.nrao.edu/~rmaddale/GBT/

Table 1. Summary of the general properties of the observing sample.

Galaxy name	RA J(2000)	Dec. J(2000)	v_{sys} (km s^{-1})	D_L (Mpc)	log L_{OH} ($L_\odot$)	log L_{H_2O} ($L_\odot$)	log L_{IR} ($L_\odot$)	log L_{Ka} (W Hz^{-1})	log $L_{0.5-2\,keV}$ ($L_\odot$)	log $L_{2-10\,keV}$ ($L_\odot$)
(1)	(2)	(3)	(4)	(5)	(6)	(7)	(8)	(9)	(10)	(11)
IRAS00509+1225	00:53:34.90	+12:41:36.0	17 658	248	2.6	–	11.9	–	10.0	10.2[C07]
NGC520	01:24:35.07	+03:47:32.7	2281	27.1	–	0.3	11.0	21.4[f]	–	–
NGC2782	09:14:05.10	+40:06:49.0	2543	38.1	–	1.2	10.6	21.4[f]	7.8	9.4[Z06]
UGC5101	09:35:51.60	+61:21:11.0	11 802	168	1.6	3.3	12.0	–	8.3	8.6[G09]
NGC3690	11:28:32.20	+58:33:51.0	3121	45.2	1.5	1.5	11.8	21.6[m]	7.5	7.5[P11]
IRAS12112+0305	12:13:45.98	+02:48:40.1	21 980	324	3.0	–	12.3	22.8[f]	7.5	7.7[G09]
NGC4258	12:18:57.50	+47:18:14.0	448	8.97	–	2.1	9.9	20.7[f]	7.3	7.5[C06]
NGC4388	12:25:46.70	+12:39:44.0	2524	39.4	–	1.2	10.8	21.2[f]	8.4	9.0[C06]
Mrk231	12:56:14.23	+56:52:25.2	12 642	181	2.9	–	12.5	23.5[m]	8.0	8.8[S11]
Mrk273	13:44:42.08	+55:53:13.0	11 326	162	2.6	–	12.2	22.8[m]	9.7	9.5[G09]
M51	13:29:52.70	+47:11:43.0	463	10.6	–	−0.1	10.6	21.2[f]	7.4	7.2[C06]
NGC5728	14:42:23.90	−17:15:11.0	2804	41.9	–	2.0	10.7	–	8.1	9.1[C10]
IRAS15250+3609	15:26:59.41	+35:58:37.3	16 535	238	2.6	–	12.0	22.5[m]	7.5	7.0[T05]
Arp220	15:34:57.24	+23:30:11.4	5434	77.2	2.6	–	12.2	22.6[m]	6.6	7.1[I11]
NGC6240	16:52:58.90	+02:24:03.0	7339	103	–	1.6	11.8	22.6[f]	8.7	8.9[G09]
IR23365+3604	23:39:01.30	+36:21:08.0	19 331	273	2.5	–	12.2	22.3[m]	7.4	8.0[T05]

Column (1): source name; columns (2) and (3): the targeted positions for the GBT observations; column (4): the heliocentric systemic velocity taken from the NED data base; column (5): the luminosity distance (calculated using cosmological parameters $H_0 = 73$ km s^{-1} Mpc^{-1}, $\Omega_M = 0.27$ and $\Omega_\Lambda = 0.73$); columns (6) and (7): the logarithm of the OH and H_2O luminosity adopted from Darling & Giovanelli (2002) and Zhang et al. (2012), respectively, but scaled for the distances listed in column (5); column (8): logarithm of the infrared luminosity, estimated using the method of Sanders & Mirabel (1996); column (9): logarithm of the radio luminosity at *Ka* band from the NED data base – '*m*' represents an estimate from a direct measurement at *Ka* band, '*f*' represents an estimate from fitting to the measurements at other radio wavelengths with a power law SED distribution. Columns (10) and (11): logarithm of the soft X-ray (0.5–2 keV) and hard X-ray (2–10 keV) luminosities, respectively, but scaled for the distances listed in column (5). The references for the X-ray luminosities (both soft and hard) are as follows: C07 – Costantini et al. (2007); Z06 – Zhang et al. (2006); G09 – González-Martín et al. (2009); P11 – Pereira-Santaella, Alonso-Herrero & Santos-Lleo (2011); C06 – Cappi et al. (2006); S11 – Singh, Shastri & Risaliti (2011); C10 – Comastri et al. (2010); T05 – Teng et al. (2005); I11 – Iwasawa et al. (2009).

instrument for such observations. For our current GBT observational data it is not possible to remove the baseline with a lower-order polynomial fit for the whole 1.25 GHz bandwidth. Instead, for each source we fitted a polynomial baseline (typically of order less than 10) over a 0.4-GHz (∼3300 km s^{-1}) frequency range centred on the redshifted sky frequency of the methanol line. This method is effective for all the observed sources with the exception of Arp 220 which has an unusually wide velocity range (∼1000 km s^{-1}) for both the class I methanol emission and other molecular lines (see Chen et al. 2015 and references therein). Because of this, the GBT methanol spectrum of Arp 220 is confused with bandpass ripples and we are unable to obtain a satisfactory spectrum from the current GBT observations. Fig. 1 shows the GBT data and data reduction method described above for the detected methanol sources. The complete figure set (11 images) are available in the online journal.

3 RESULTS

We initially identified the sources with integrated emission (S_{int}) at least three times stronger than the rms noise limit for the integrated intensity ΔS. We calculate ΔS using the formula $\Delta S = \sigma_{rms}(\Delta W \times \Delta v_{res})^{1/2}$, where σ_{rms} is the baseline rms noise level, Δv_{res} is the velocity resolution of the observations (about 20 km s^{-1} after spectral smoothing; see below) and ΔW is the full velocity width over which the integrated intensity is calculated (here, we use 2.5 times the full width at half-maximum – FWHM – linewidth of the methanol spectrum, Δv from the Gaussian fitting). Furthermore, we undertook a series of additional tests for each of the spectral features identified in the initial search: (1) whether the line feature is visible in only one of the polarizations; (2) whether, when the data is divided into two or three time intervals, the feature is present in only one of these; (3) for sources with a systemic velocity of less than 3000 km s^{-1}, we checked whether the feature was present in only one of spectrometers 3 and 4 (see Section 2). Sources which failed any of these three tests were discarded as non-detections, since if true weak emission is present just above the detection threshold then it should not be readily observed in a single polarization (case 1) or a significantly shorter time interval (case 2). We found that in case 3 all the six sources with a systemic velocity of less than 3000 km s^{-1} (see Table 1) show similar characteristic of either detection or non-detecion in both the spectrometers. Therefore if the performance of the backend and correlator is consistent for all four of the VEGAS spectrometers, the detected features from the other sources are also unlikely to be artefacts from the system.

Based on these criteria, we tentatively detected 36.2-GHz class I methanol emission towards 10 of the 16 targeted sources from the GBT survey (note that Arp220 is not included in this group; see below). The 36.2-GHz methanol spectrum of these 10 sources is shown in Fig. 2. The spectra we show were smoothed with a 24-channel boxcar (2.3 MHz; corresponding a velocity resolution of about 20 km s^{-1}). The parameters of Gaussian fits to the 36.2-GHz spectral features are given in Table 2. The peak flux densities of the emission determined from the Gaussian fits range between ∼2 and 8 mJy. The integrated flux densities range from 0.1 to 5.2 Jy km s^{-1}. The majority of the galaxies show a single component in the methanol spectrum, but two sources (IRAS00509+1225 and Mrk231) show three spectral components (see Fig. 2). The measured FWHM linewidth of the individual spectral components ranges between 40 and 320 km s^{-1} with a mean of 200 km s^{-1}.

The velocity of the peak for the spectral components of the tentative detections are offset with respect to the systemic velocity for many sources (from a few hundred to 1000 km s^{-1}). The velocity

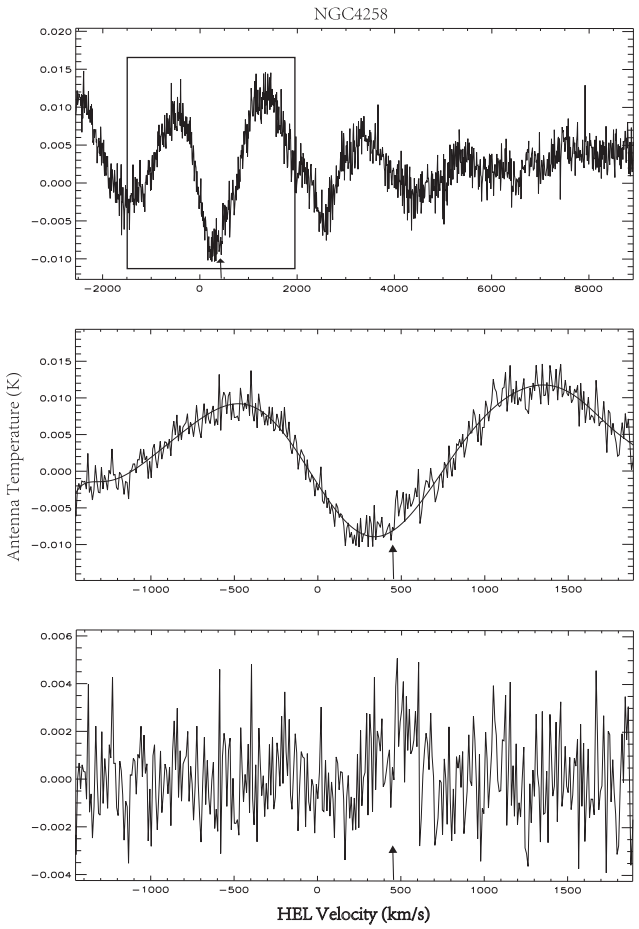

Figure 1. The GBT data and data reduction procedures of the detected methanol sources. The upper panel shows the original spectrum for the spectrometer covering the 36.2-GHz methanol transition towards the source NGC4258. The middle panel shows the polynomial baseline fitting of the spectral range indicated by the box in the upper panel. The lower panel shows the final spectrum. The upward arrow marks the systemic velocity of the target galaxy. These shown spectra were binned with a 12-channel boxcar (1.1 MHz, corresponding to a velocity resolution of ∼10 km s^{-1}.)

offset for each source is listed in Table 2. We extracted information on the velocity range of the H I emission and OH or H_2O megamasers from the literature and show these in Fig. 2. We can see that most of the tentative detections are located within or near the edge of the spectral ranges of H I emission and OH or H_2O megamasers, suggesting that these signals are associated with the host galaxies. However, in two sources (Mrk231 and IRAS23365+3604), there are significant offsets of the methanol spectral features from the velocity range observed in other species and the systemic velocity. We suggest that the large velocity offsets observed in the methanol emission may be due to it being associated with galactic-outflow-driven shocks (we discuss this further in Section 4.2). However, it is possible that some of the spectral components we have attributed to methanol emission may be artefacts resulting from the poor initial baselines and the baseline removal process. For this reason we have further divided the tentative detections into as being either 'likely' or 'possible', based on the following criteria: the likely group includes sources with one or more spectral components $\geq 7\sigma$ (i.e. SNR $\geq$ 7 listed in column 5 of Table 2), and sources with one or more components $\geq 5\sigma$ with a peak velocity within 250 km s^{-1} of the systemic velocity. Among the 10 tentative detections from the GBT survey, six meet one of these criteria and are classified into the likely group, with the remaining four sources considered to be the possible group (see Table 2). However, more sensitive observations are required to confirm all these tentative detections in both the likely and possible groups.

We have calculated the isotropic luminosity of the methanol emission for each of tentative sources:

$$L_{\rm methanol} = 4\pi D_{\rm L}^2 S_{\rm int} \left(\frac{1}{c}\right)\left(\frac{\nu_0}{1+z}\right), \quad (1)$$

where $D_{\rm L}$ is the luminosity distance of the galaxy (see Table 1) and ν_0 is the rest frequency of the 36.2-GHz methanol transition. The derived methanol luminosities are in the range of 1–6000 $L_\odot$.

As stated in Section 2, the methanol emission from Arp 220 is confused by the bandpass ripples and we are not able to disentangle the two in the current GBT observations. Because of this we have used the 36.2-GHz methanol luminosity measurement from our previous ATCA observations of Arp 220 (2300 $L_\odot$; see Chen et al. 2015) in the following analysis.

In addition to the above 10 tentative detections we detected a possible narrow methanol absorption feature in IRAS22365+3004 (with a linewidth of ∼40 km s^{-1}; shown in Fig. 2) and possible broad methanol absorption from Mrk273. The methanol absorption spectrum of Mrk273 is also shown in Fig. 2. The velocity of the greatest absorption is close to the systemic velocity in IRAS22365+3004 and Mrk273. Gaussian fitting to the absorption profile of Mrk273 shows that it has a linewidth of approximately 500 km s^{-1}. This broad absorption is likely due to absorption of the background radio continuum of the nuclei of the galaxies, and traces more widespread gas foreground of the nuclei. Methanol absorption from the 6.7-GHz class II transition has previously been detected in Arp 220 (Salter et al. 2008) and NGC 3079 (Impellizzeri et al. 2008). In Arp 220 and NGC 3079 the 6.7-GHz methanol absorption presumably dominates because its production is overall more effective on large scales in these galaxies compared to any maser emission from this transition. However, we cannot completely exclude the possibility that the absorption signature in Mrk273 is due to baseline ripples. This requires confirmation observations and in this paper, we only show the possible absorption spectra and do not consider them further in our discussions.

For the remaining four galaxies (NGC 2782, NGC 6240, M51 and UGC5101), we detected neither 36.2-GHz methanol emission nor absorption. We give upper limits on the integrated flux density and luminosity of the methanol emission for these two sources which are computed from the baseline rms noise ($\sigma_{\rm rms}$) of the non-detection spectrum, assuming a line profile of linewidth Δv = 200 km s^{-1} and height $3\sigma_{\rm rms}$.

4 DISCUSSION

Although we only achieved tentative detections from the GBT survey due to the large baseline ripples of the observations, some analysis is still worthwhile in order to investigate relationships between properties of class I methanol megamasers and other wavelength ranges of the host galaxies, and the pumping conditions for the methanol megamasers. In the following discussions we consider all tentative detections in both the likely and possible groups in our statistical analysis, as otherwise the sample size is too small for investigation; however, for clarity we distinguish the two groups using different symbols in the plots.

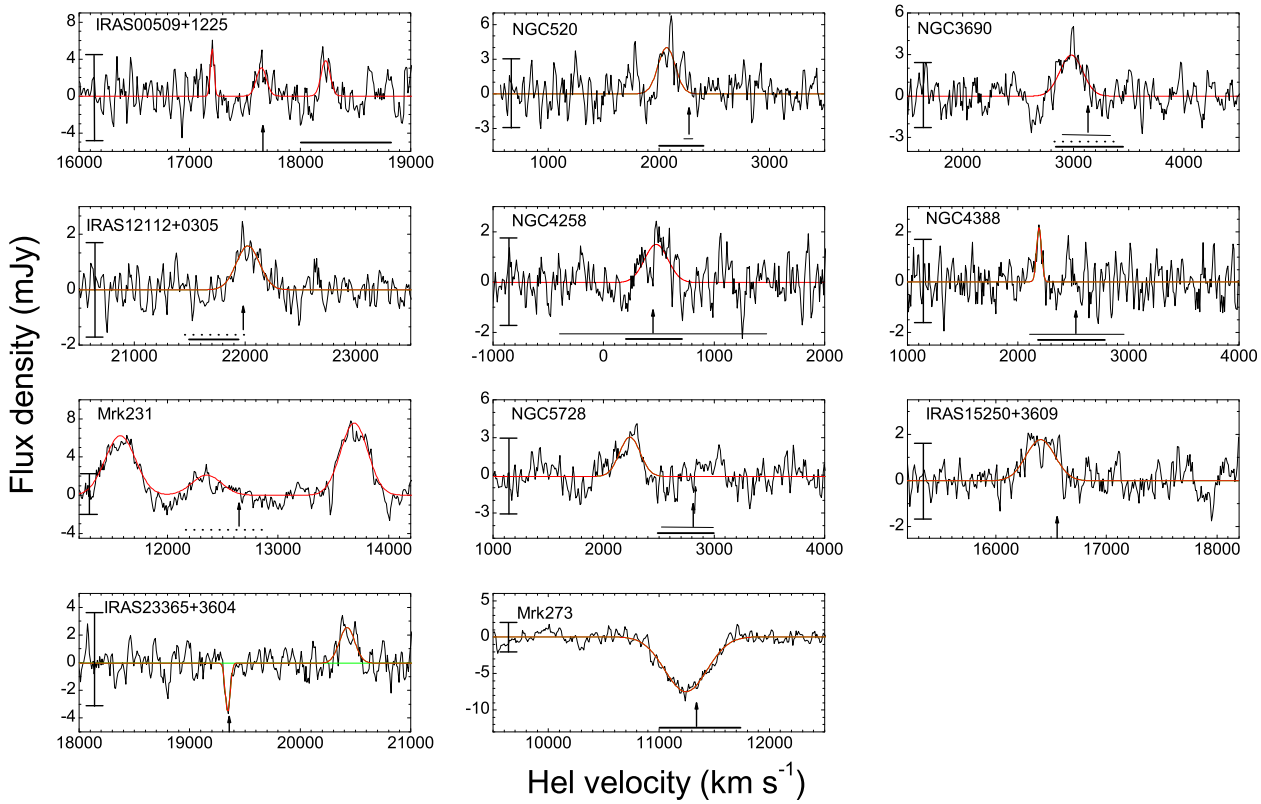

Figure 2. Spectra of the 36.2-GHz class I methanol emission and absorption detected in the GBT survey. The 3σ significance level of each spectrum is given with vertical solid line. The red solid lines represent the profiles of Gaussian fitting of individual maser feature. The spectral ranges of H I, OH and H_2O megamasers are denoted by thick solid, thick dashed, and thin solid lines, respectively, if they are available from the literature or data bases. The upward arrow marks the systemic velocity of the source.

4.1 The relationship between methanol emission and that observed at other wavelengths

Methanol–X-ray: Chen et al. (2015) show that the spatial distribution of the 36.2-GHz class I methanol megamaser in Arp 220 is closely correlated with the soft X-ray emission. Assuming that the X-ray emission reflects the cosmic ray intensity, they argue that cosmic rays are responsible for the production of the class I methanol megamasers, which has been used to explain the enhanced class I methanol maser emission in the central regions of the Milky Way (Yusef-Zadeh et al. 2013) and NGC 253 (Ellingsen et al. 2014). We have used the published literature (see Table 1) to obtain X-ray data for our observing sample. The distribution of 36.2-GHz methanol luminosity versus soft (0.5–2.0 keV) and hard (2.0–10 keV) X-ray luminosity is presented in Fig. 3(a) (on a log–log scale). However, no significant correlation between methanol luminosity and X-ray luminosity is observed for our surveyed sample. This demonstrates that the luminosity of 36.2-GHz class I methanol masers are not related to the integrated X-ray emission of the galaxies. Chen et al. (2015) suggested that the class I methanol megamaser in Arp 220 may be produced either by galactic-outflow-driven shocks or cosmic rays. The lack of a correlation between the methanol and X-ray luminosity supports the hypothesis that galactic-outflow-driven shocks play a key role in the production of class I methanol megamasers (we further discuss this in Section 4.2).

Methanol–IR: Fig. 3(b) shows the relationship between 36.2-GHz class I methanol luminosity and IR luminosity of the host galaxy for our survey sample plotted on a log–log scale. We find that $L_{\rm methanol}$ and $L_{\rm IR}$ are well-correlated ($R = 0.92$). A straight-line fit gives the relation $\log L_{\rm methanol} = (1.36 \pm 0.18) \log L_{\rm IR} - (13.47 \pm 2.08)$. However, since both $L_{\rm methanol}$ and $L_{\rm IR}$ are related to the distance $D_{\rm L}$, we expect there to be a partial correlation due to Malmquist bias. We follow the procedure used by Darling & Giovanelli (2002) to account for the partial correlation caused by Malmquist bias. In our sample, $L_{\rm methanol}$ and $L_{\rm IR}$ are correlated with distance with correlation coefficients of the following: $R(L_{\rm IR}, D_{\rm L}) = 0.86$, and $R(L_{\rm methanol}, D_{\rm L}) = 0.88$. Calculating the partial correlation coefficient between methanol and IR luminosity at fixed distance we find that we still have a significant $L_{\rm methanol}$–$L_{\rm IR}$ correlation of $R = 0.68$. The corrected slope (1.01 ± 0.18) in the $L_{\rm methanol}$–$L_{\rm IR}$ relation is shallower than the simple fit slope (1.36). Therefore we find $L_{\rm methanol} \propto L_{\rm IR}$.

The statistical analysis of a large sample of OH megamasers undertaken by Darling & Giovanelli (2002) found that the OH luminosity increases with the IR luminosity of the host galaxy as follows: $L_{\rm OH} \propto {L_{\rm IR}}^{1.2}$. On the assumption that the OH megamaser is pumped by the IR radiation field and amplifies the background radio continuum emission, which is itself proportional to the IR radiation from star-forming regions, the observed OH maser output is expected to be $L_{\rm OH} \propto L_{\rm IR} L_{1.6\,\rm GHz} \propto {L_{\rm IR}}^2$. As the observed slope of the relationship between $L_{\rm OH}$ and $L_{\rm IR}$ is 1.2 (smaller than 2), Darling & Giovanelli (2002) suggested that OH megamasers contain a mixture of saturated and unsaturated emission. Here we find a perfectly linear dependence between $L_{\rm methanol}$ and $L_{\rm IR}$, suggesting that the pumping mechanism for methanol megamasers is likely to be different from that for OH megamasers as the power-law exponent for $L_{\rm methanol}$–$L_{\rm IR}$ is different from that for $L_{\rm OH}$–$L_{\rm IR}$ even considering the uncertainty. In particular, for the two extragalactic

Table 2. Observed properties of 36.2-GHz class I methanol emission.

Galaxy name	Gaussian fit $v_{\rm Hel}$ (km s^{-1})	Δv (km s^{-1})	S (mJy km s^{-1})	SNR	$v_{\rm off}$ (km s^{-1})	L (L$_\odot$)
(1)	(2)	(3)	(4)	(5)	(6)	(7)
Likely detections:						
NGC520	2070(10)	185(23)	785(95)	5.0	−210	22
NGC3690	2976(23)	221(20)	692(17)	8.6	−150	53
IRAS12112+0305	22 020(16)	232(16)	352(13)	5.7	40	1300
NGC4258	476(26)	252(21)	405(18)	5.4	28	1
Mrk231	11 573(18)	323(25)	2140(145)	21.9	−1070	6100
–	12 354(24)	316(18)	707(143)	7.3	−290	–
–	13 689(17)	290(24)	2340(137)	25.3	1040	–
IRAS15250+3609	16 403(20)	301(50)	588(90)	7.1	−130	1200
Possible detections:						
IRAS00509+1225	17 201(6)	42(20)	216(80)	3.2	−460	2100
–	17 648(20)	104(50)	347(142)	3.0	10	–
–	18 229(15)	90(35)	396(136)	3.6	570	–
NGC4388	2190(10)	50(14)	118(43)	3.5	−330	7
NGC5728	2238(15)	217(36)	727(114)	6.6	−570	48
IR23365+3604	20 425(18)	164(24)	448(59)	4.3	1090	1200
Non-detections:						
NGC2782	–	–	–	–	–	<22
NGC6240	–	–	–	–	–	<280
M51	–	–	–	–	–	<2.5
UGC5101	–	–	–	–	–	<430

Column (1): source name. Columns (2)–(4): the velocity at peak $v_{\rm Hel}$, the line FWHM Δv and the integrated intensity S of each maser feature estimated from Gaussian fits to the 36.2-GHz class I methanol maser lines. The formal error from the Gaussian fit is given in parenthesis. Column (5): the signal-to-noise ratio for the integrated flux of each spectral feature. Column (6): the offset of the peak velocity of the spectral feature with respect to the systemic velocity of the source. Column (7): the total integrated luminosity of the maser spectrum obtained from summing all maser features in each source.

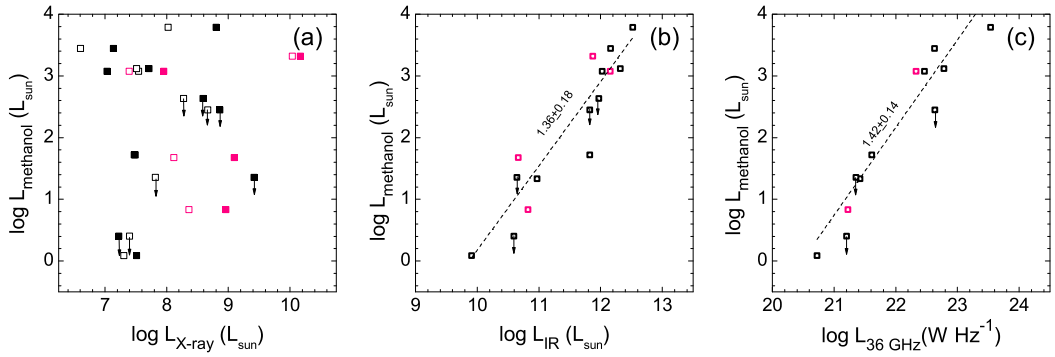

Figure 3. Relationships between the luminosity of the 36.2-GHz methanol megamasers detected from our GBT survey and that observed in other wavelength ranges for the host galaxies: (a) methanol versus soft X-ray emission (0.5–2 keV; marked with open squares) and hard-X-ray emission (2–10 keV; marked with filled squares) relations; (b) methanol versus IR; (c) methanol versus radio (36 GHz) relation. In the three panels, the likely and possible detections are indicated using black and red symbols, respectively. Upper limits for the methanol luminosity are indicated by downward arrows for four non-detection sources (M51, NGC 2782, NGC 6240 and UGC5101; see text). Dotted lines are fits to the data labelled by their slopes. No fit has been undertaken for the methanol versus X-ray relationship due to the lack of significant correlation between these two quantities.

class I methanol masers where high-resolution line and continuum data is available (NGC 253 and Arp 220) the maser emission is observed to be significantly offset from the continuum emission (Ellingsen et al. 2014; Chen et al. 2015). This suggests that it is unlikely that there is significant amplification of the background continuum emission in luminous extragalactic class I methanol masers.

Methanol–Radio: to further investigate the relationship between the luminosity of the methanol and radio continuum emission discussed above, we compare the distribution of their luminosities (on a log–log scale) in Fig. 3(c). In Table 1 we give the flux densities at *Ka* band that have been directly measured for six galaxies in the survey sample (extracted from the NASA/IPAC Extragalactic Database – NED). For a further seven galaxies we have estimated the flux density at 36 GHz from a power-law fit to the spectral energy distribution (SED) at lower frequencies, while for the remaining three sources, there is insufficient data at lower frequencies to obtain a reliable power-law fitting to the SED. From these data we find that $L_{\rm methanol}$ and $L_{36\,\rm GHz}$ are well-correlated with each other – $R(L_{\rm methanol}, L_{36\,\rm GHz}) = 0.96$ – and with distance: $R(L_{\rm methanol}, D_{\rm L}) = 0.86$, and $R(L_{36\,\rm GHz}, D_{\rm L}) = 0.82$. For the uncorrected fit the relationship is $L_{\rm methanol} = (1.42 \pm 0.14) \log L_{36\,\rm GHz} - (29.1 \pm 3.1)$,

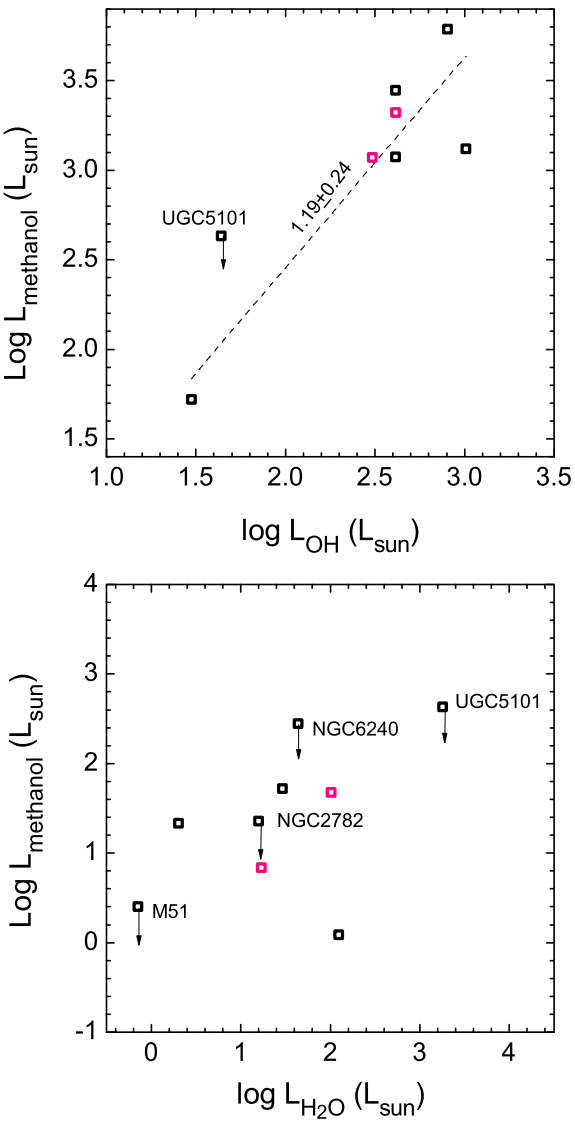

Figure 4. Relationships between the luminosity of the 36.2-GHz methanol megamasers and the OH (upper panel) and H_2O megamasers (lower panel) in the same host galaxies. Downward arrows mark the upper limits of the 36-GHz methanol emission for non-detection sources M51, NGC 2782, NGC 6240 and UGC5101. The dotted line is the best fit to the methanol–OH dependence.

while the fit after correction for Malmquist bias remains significant ($R = 0.88$) and has a slope of 1.30. This demonstrates that there is a good correlation between the high-frequency radio continuum and methanol maser luminosity. We found that there is also a good correlation between the radio continuum and IR luminosity in the detected methanol sources: $L_{36\,\mathrm{GHz}} \sim 0.94\,L_{\mathrm{IR}}$. Therefore the Methanol–Radio correlation may not represent a causal relationship because both the L_{methanol} and $L_{36\,\mathrm{GHz}}$ are similarly correlated with a common third factor (i.e. IR luminosity).

Methanol–OH or H_2O masers: possible relationships between the luminosity of the methanol and the associated OH and/or H_2O megamasers are investigated in Fig. 4. We find a statistically significant correlation between the methanol and OH maser emission: $L_{\mathrm{methanol}} = (1.19 \pm 0.24) \log L_{\mathrm{OH}} - (0.09 \pm 0.62)$, ($R = 0.89$), although this is derived from a small sample of sources. As the OH megamasers trace enhanced star formation in circumnuclear starburst regions, the correlation between OH and methanol megamasers suggests that the methanol megamasers are also associated with starburst activity. No significant correlation was found between the luminosity of the methanol and H_2O megamaser emission (Fig. 4). Typically H_2O megamasers are observed to trace circumnuclear accretion discs or inner jets in the nuclear region of an active galaxy; thus the absence of a correlation with the methanol luminosity suggests that the methanol megamasers are not associated with the discs or inner jets. It is also consistent with the observations of Arp 220 and NGC 253 which show the class I methanol emission offset from the centre of the host galaxy.

4.2 Comparison of methanol detections in OH and H_2O megamaser galaxies

In the surveyed sample, all but one of the OH megamaser galaxies are observed to have an associated methanol megamaser or absorption (Mrk273). The only exception is UGC5101 which also shows H_2O megamaser emission. The other three non-detections are also from the H_2O megamaser sources M51, NGC 2782 and NGC 6240. OH megamasers are known to be associated with starburst galaxies, and the possible correlation between the methanol and OH luminosity derived in Section 4.1 supports the suggestion that class I methanol megamasers are associated with strong starburst activity. Although we find no significant correlation between methanol and H_2O luminosity (see Section 4.1), methanol emission is also commonly found in the sample of H_2O megamasers. This can be understood if the H_2O megamaser sample is also associated with starburst activity. Examination of the properties of the host galaxies of the OH and H_2O megamaser sources in our target sample shows that they are predominantly luminous IR galaxies with $L_{\mathrm{IR}} > 10^{11}\,\mathrm{L}_{\odot}$, indicating the presence of significant star formation activity. One exception to this line of reasoning is presented by NGC 6240, which is a prototypical luminous IR galaxy with $L_{\mathrm{IR}} \approx 6 \times 10^{11}\,\mathrm{L}_{\odot}$, but which shows no class I methanol megamaser emission. Based on the relationships between the methanol and OH megamaser luminosity and that of the host galaxy (see Section 4.1), we would expect it to show both OH and methanol emission; however, neither are detected. This suggests that there is something different about NGC 6240 compared to the majority of the luminous IR galaxies, perhaps it is in the declining phase of its starburst where it has exhausted the molecular reservoir, but the final epoch of star formation maintains the extreme IR emission (see Lo 2005).

4.3 Class I methanol megamasers as tracers of AGN feedback

The GBT observations show that there are some sources where the velocity of the tentatively detected emission is significantly offset (between a few hundred and 1000 km s^{-1}) from the systemic velocity of the host galaxy (see Fig. 2). Large velocity offsets of around 1000 km s^{-1} are detected in two sources Mrk 231 and IRAS23365+3604 (see Table 2). To more directly investigate the observed velocity offsets in Fig. 5 we compare the spectra of the detected 36.2-GHz class I methanol emission with those of the dense gas tracer HCO^+ 1–0 (89.2 GHz) towards three galaxies, NGC 4258, NGC 4388 and Mrk231. The HCO^+ spectra are from the recent survey of dense gas tracers in extragalactic sources made with the IRAM 30 m telescope (Wang et al., in preparation). The HCO^+ emission traces the dense gas for each of the host galaxies and for these three sources shows that the velocity range of the methanol emission is similar to that of the HCO^+ in NGC 4258, but is significantly offset in NGC 4388 and Mrk 231. The methanol

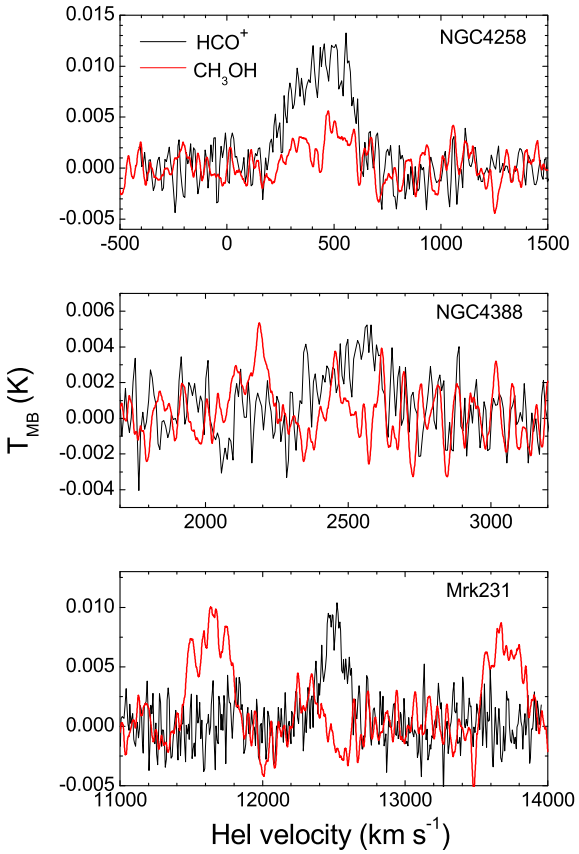

Figure 5. Comparison of spectra of the 36.2-GHz class I methanol detected in the GBT survey with HCO^+ 1–0 spectra detected with IRAM 30 m from our extragalactic dense molecular line surveys.

emission in NGC 4388 is blueshifted, with the strongest component ∼400 km s^{-1} offset with respect to the HCO^+ peak. Towards Mrk 231 three methanol spectral features are observed, two of which are blue- and redshifted by approximately 1000 km s^{-1} with respect to the systemic velocity, and the third being near the systemic velocity (overlapping the blue line-wing emission observed in HCO^+). A similar partial overlap of the class I methanol emission and the line wing of a dense gas tracer is also observed in the Seyfert galaxy NGC 1068 (Wang et al. 2014) where the 84.5-GHz class I methanol emission overlaps with the line wing of the HCN emission. The large velocity offset (up to 1000 km s^{-1}) of methanol emission with respect to dense molecular gas tracers has not previously been observed. It suggests that there are different production mechanisms for class I methanol masers and dense gas tracers. The dense gas tracers are typically associated with star-forming giant molecular cloud (GMC) cores and are mainly concentrated in the central regions (<1 kpc) of the host galaxies (Gao & Solomon 2004). The velocity range of extragalactic dense gas tracers is typically a few hundred km s^{-1} (<500 km s^{-1}), which is consistent with stellar processes associated with star formation when the kinematics of galactic rotation, infall, outflow and turbulence within the star-forming GMC are considered. The much larger velocity offset of some of the methanol emission requires a different mechanism, such as shocks driven by galactic-scale outflows with large velocities (a few hundred to 1000 km s^{-1}). These high-velocity outflows may be as a result of AGN feedback on their host galaxies (see below), or from nuclear starburst activity. However, we note that the features with large velocity offsets identified in our observations may correspond to some small baseline ripples. Additional, more sensitive, observations unaffected by baseline ripples are required to confirm (or otherwise) the spectral features with significant velocity offsets.

Recent observations of massive, highly energetic, and large (kpc)-scale outflows in local AGN hosts and ULIRGs (e.g. Cicone et al. 2012, 2014; Tombesi et al. 2015) provide strong evidence for winds from the black hole accretion disc providing feedback. These molecular outflows show high-velocity components (e.g. >500 km s^{-1}), which are difficult to reconcile with stellar processes in large masses of cold molecular gas. In our sample the most extreme source is Mrk231, for which millimetre CO observations show a high-velocity molecular outflow with a velocity of up to 1000 km s^{-1} (Cicone et al. 2012). Thus the velocity offsets of the blue- and redshifted methanol emission tentatively detected in Mrk 231 are consistent with the high-velocity outflow components, supporting the hypothesis that class I methanol megamasers are produced in galactic-scale outflows. This suggests that class I methanol megamasers may be used as a new tool for investigating AGN feedback processes. The interferometric observations of Arp 220 also reveal that the class I methanol maser emission is excited in regions of galactic outflow on scales of a few kpc, as traced by the diffuse soft-X-ray emission (Chen et al. 2015).

The sources in our sample show methanol emission with a wide range of velocity offsets with respect to the systemic velocity of the host galaxy. In some sources the velocity is similar to the systemic, while in others it is offset by a few 100–1000 km s^{-1}. This suggests that the observed methanol emission is associated with outflows at a range of different angles with respect to the line of sight. Since we have detected methanol emission from a large fraction of our target sample, this implies that we are not limited to a particular geometry (unless that geometry is an inherent bias in the target sample). For example, NGC 4258 is a very-well-studied Seyfert 2 located in a near-edge-on disc galaxy and hence outflows from the nuclear region will be nearly perpendicular to the line of sight. So we would not expect to observe a significant velocity offset between the methanol emission and the systemic velocity in this source (which is consistent with the results shown in Fig. 5).

Considering the discussion here and that from Section 4.1, we argue that the observational evidence to date suggests that class I methanol megamasers form in galaxies with significant starburst activity and strong molecular outflows. They provide a potential probe of feedback process of these active galaxies via wind-driven outflows. However, further high-resolution observations of class I methanol megamasers in a larger sample are required to clarify the association between the methanol megamasers and the outflows and determine how they trace the AGN feedback process.

5 CONCLUSIONS

Using the GBT, we have performed a systematic search for class I methanol megamasers in the 36.2 GHz transition towards a sample of 16 galaxies which show emission of diffuse soft X-ray and, either OH or H_2O megamasers. 11 sources show tentative detections in the surveyed sample. A further more sensitive observation (with rms < 1 mJy) with better baselines are required for clarifying these tentative detections. However, investigation of possible relationships between these tentative detections of methanol emission with that in other wavelength ranges of host galaxies shows significant correlations between the methanol luminosity, and that of the IR and radio luminosities of the host galaxies. The observed relationship, $L_{\rm methanol} \propto L_{\rm IR} \propto L_{36\,\rm GHz}$, suggests that the methanol emission

may be related to the starburst activity of the host galaxy. This is also supported by the evidence for a significant correlation between the methanol and OH megamaser luminosities and the absence of any correlation between methanol and H_2O luminosities. This is consistent, since the OH megamasers are known to trace starburst activity, while H_2O megamasers trace the accretion disc and jets of AGNs.

Our previous interferometric observations showed that class I methanol megamasers are spatially correlated with the diffuse X-ray emission in Arp 220, suggesting that they may be produced from either galactic-outflow-driven shocks and/or cosmic rays. The current GBT survey for a larger sample of sources shows no correlation between the methanol and X-ray luminosities of the host galaxies, suggesting that the methanol megamasers are not related to galactic-scale high-energy cosmic rays. In addition, the current tentative detections show that some sources have high-velocity spectral components offset by between a few hundred and 1000 km^{-1} from the systemic velocity of the host galaxy. High-velocity features such as this are thought to be associated with galactic-outflow driven by winds from AGN feedback. In combination, the observational evidence to date, suggests that class I methanol megamasers provide a potential tool for investigating the starburst and feedback processes of active galaxies.

ACKNOWLEDGEMENTS

We are grateful to Dr Adam Kobelski and Dr Dan Perera for their assistance during the GBT observations. We made use of the NASA/IPAC extragalactic Database (NED). This work was supported by the National Natural Science Foundation of China (11590781, 11590784, 11133008 and 11273043), the Strategic Priority Research Program of the Chinese Academy of Sciences (CAS; grant no. XDA04060701), Key Laboratory for Radio Astronomy, CAS. We made use of the facilities at Greenbank Telescope (GBT).

REFERENCES

Baan W. A., Wood P. A. D., Haschick A. D., 1982, ApJ, 260, L49
Batrla W., Menten K. M., 1988, ApJ, 329, L117
Brassington N. J., Ponman T. J., Read A. M., 2007, MNRAS, 377, 1439
Breen S. L., Caswell J. L., Ellingsen S. P., Phillips C. J., 2010, MNRAS, 406, 1487
Cappi M. et al., 2006, A&A, 446, 459
Caswell J. L. et al., 2010, MNRAS, 404, 1029
Chen X., Ellingsen S. P., Shen Z. Q., Titmarsh A., Gan C.-G., 2011, ApJS, 196, 9
Chen X., Ellingsen S. P., Gan C. G., Xu Y., Shen Z. Q., 2014, Chin. Sci. Bull., 59, 1066
Chen X., Ellingsen S. P., Baan W. A., Qiao H. Q., Li J., An T., Breen S. L., 2015, ApJ, 800, L2
Cicone C., Feruglio C., Maiolino R., Fiore F., Piconcelli E., Menci N., Aussel H., Sturm E., 2012, A&A, 543, A99
Cicone C. et al., 2014, A&A, 562, 21
Comastri A., Iwasawa K., Gilli R., Vignali C., Ranalli P., Matt G., Fiore F., 2010, ApJ, 717, 787
Costantini E., Gallo L. C., Brandt W. N., Fabian A. C., Boller T., 2007, MNRAS, 378, 873
Darling J., Giovanelli R., 2002, AJ, 124, 100
Ellingsen S. P., 2006, ApJ, 638, 241
Ellingsen S. P., Breen S. L., Caswell J. L., Quinn L. J., Fuller G. A., 2010, MNRAS, 404, 779
Ellingsen S. P., Chen X., Qiao H. Q., Baan W., An T., Li J., Breen S. L., 2014, ApJ, 790, 28
Gao Y., Solomon P. M., 2004, ApJ, 606, 271
González-Martín O., Masegosa J., Mírquez I., Guainazzi M., Jiménez-Bailón E., 2009, A&A, 506, 1107
Green J. A. et al., 2008, MNRAS, 385, 948
Green J. A. et al., 2009, MNRAS, 392, 783
Impellizzeri C. M. V., Henkel C., Roy A. L., Menten K. M., 2008, A&A, 484, L43
Iwasawa K., Sanders D. B., Evans A. S., Mazzarella J. M., Armus L., Surace J. A., 2009, ApJ, 695, L103
Kandalyan R. A., 2003, A&A, 404, 513
Li J. J. et al., 2012, ApJ, 749, 47
Lo K. Y., 2005, ARA&A, 43, 625
Menten K. M., 1991, ApJ, 380, L7
Miyoshi M., Moran J., Herrnstein J., Greenhill L., Nakai N., Diamond P., Inoue M., 1995, Nature, 373, 127
Pereira-Santaella M., Alonso-Herrero A., Santos-Lleo M., 2011, A&A, 535, 93
Salter C. J., Ghosh T., Catinella B., Lebron M., Lerner M. S., Minchin R., Momjian E., 2008, AJ, 136, 389
Sanders D. B., Mirabel I. F., 1996, ARA&A, 43, 749
Singh V., Shastri P., Risaliti G., 2011, A&A, 532, 84
Sjouwerman L. O., Murray C. E., Pihlström Y. M., Fish V. L., Araya E. D., 2010, ApJ, 724, L158
Teng S. H., Wilson A. S., Veilleux S., Young A. J., Sanders D. B., Nagar N. M., 2005, ApJ, 633, 664
Tombesi F., Meléndez M., Veilleux S., Reeves J. N., González-Alfonso E., Reynolds C. S., 2015, Nature, 519, 436
Voronkov M. A., Caswell J. L., Ellingsen S. P., Sobolev A. M., 2010, MNRAS, 405, 2471
Wang J. Z., Zhang J. S., Gao Y., Zhang Z.-Y., Li D., Fang M., Shi Y., 2014, Nature Commun., 5, 5449
Yusef-Zadeh F., Cotton W., Viti S., Wardle M., Royster M., 2013, ApJ, 764, L19
Zhang J. S., Henkel C., Kadler M., Greenhill L. J., Nagar N., Wilson A. S., Braatz J. A., 2006, A&A, 450, 933
Zhang J. S., Henkel C., Guo Q., Wang J., 2012, A&A, 538, 152

SUPPORTING INFORMATION

Additional Supporting Information may be found in the online version of this article:

A complete figure set (11 images) for Fig. 1 – The GBT data and data reduction procedures of the detected methanol sources. (http://www.mnras.oxfordjournals.org/lookup/suppl/doi:10.1093/mnras/stw680-/DC1).

Please note: Oxford University Press is not responsible for the content or functionality of any supporting materials supplied by the authors. Any queries (other than missing material) should be directed to the corresponding author for the paper.

This paper has been typeset from a TEX/LATEX file prepared by the author.